ELM Milestone Progress Report
Third Quarter FY06
June 30, 2006

D. Brennan, J. Breslau, S. Kruger, D. Schnack, C. Sovinec, H. Strauss, L. Sugiyama with support from the NIMROD and M3D Teams.[1]

Executive Summary:
In this report we present the successful completion of the 2006 Q3 milestone. The statement of the milestone is as follows: Q3 (June 30,2006) *Incorporate refinements from Q1 (equilibria) and Q2 (increased realism of DIII-D geometry and profiles) into nonlinear scoping studies.* Studies are presented with both the NIMROD and M3D codes. Both codes have now demonstrated the stabilizing effect of the 2-fluid extended MHD terms and have developed algorithms to overcome the problem of negative densities occurring in the nonlinear regime. It has been shown that toroidal velocity shear can reduce the severity of the nonlinear evolution of the mode. The two codes are in qualitative agreement on the relative stability of the two targeted DIII equilibrium. These physics and scoping studies and algorithmic improvements will contribute to the successful completion of the remaining 2006 milestones.

Section 1 Studies with the NIMROD Code

In preparation for the milestone at the end of the fiscal year, the team has 1) studied the linear stability of realistic equilibria with the two-fluid model, 2) developed a nonlinear numerical diffusivity to improve performance with strong flow perturbations, and 3) performed parallel nonlinear MHD computations with equilibrium flow. Here, we report on each of these activities.

1.1 Two-fluid linear effects with Q2 equilibrium

Magnetohydrodynamic equilibria were generated from laboratory measurements of DIII-D discharges 113207 and 113317 during the previous quarter's milestone activities. Profiles of particle number density were produced, in addition to profiles of fields that appear directly in the force-balance equation. During this quarter, we have performed linear computations using both the resistive MHD model and the two-fluid model with Hall effect and gyroviscosity for the 113317 profiles shown in Fig. 1.1 The linear growth rate spectrum for the MHD model is peaked at n=12 with modes $5 \le n \le 20$ being unstable, as shown in Fig. 1.2. The peak growth rate is 2.3×10^5 s^{-1}. This indicates that the respective equilibrium is well above the threshold for ideal linear instability. In the experiment, the stability boundary is crossed and growth rates increase with time. With the reconstruction produced from data measured just before the nonlinear ELM event, the linear modes are robustly unstable.

Recent advances in the NIMROD algorithm allow us to model drift effects associated with the Hall electric field and gyroviscosity. The linear two-fluid results for the reconstructed 113317 equilibrium are plotted together with the MHD results in Fig. 1.2. The drift effect is clearly stabilizing to the largest mode numbers while the lower mode numbers are weakly affected. Conventional wisdom holds that two-fluid effects are stabilizing at large n-values [Rogers, B.N. and Drake, J.F., Phys. Plasmas **6**, 2797 (1999)], and this is often cited to explain

[1] Edited by S. C. Jardin (jardin@pppl.gov)

experimental observations that very high mode numbers are not observed in ELM events. The eigenfunctions for the different plasma models are similar, but the two-fluid result includes a resonance effect associated with the poloidal drift—similar to an effect that is also observed with toroidal flow shear in MHD—see Section 1.3.

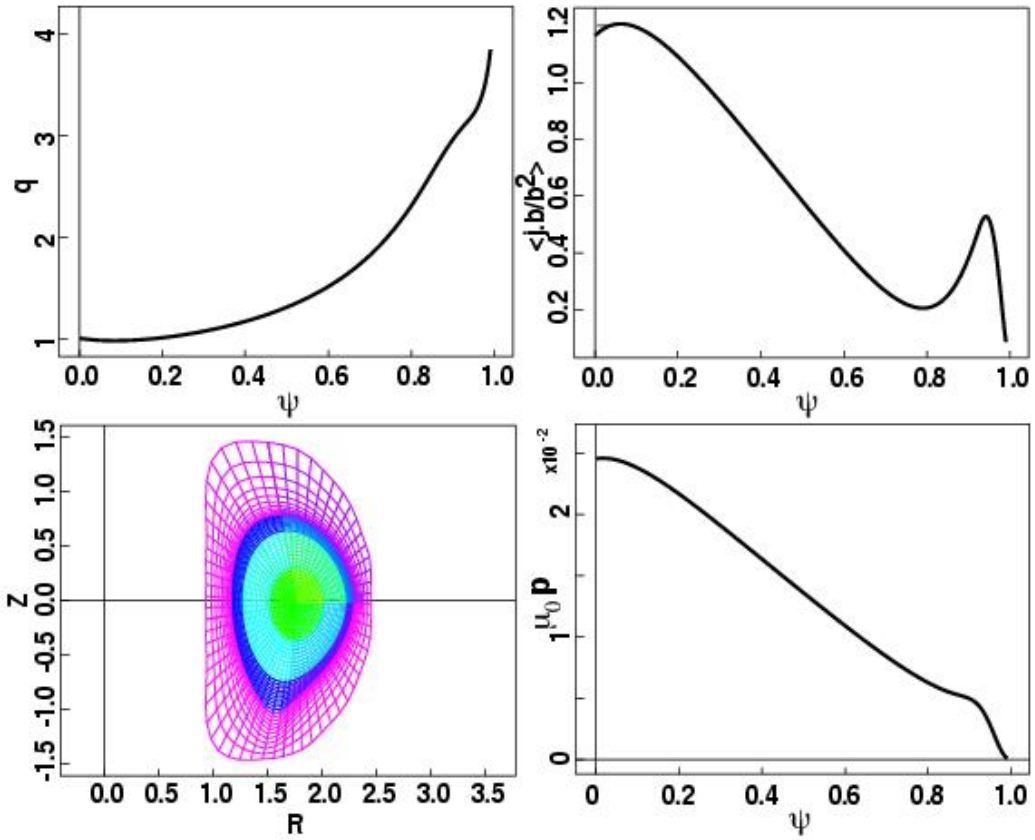

Figure 1.1. Profiles of safety factor (q, top left), parallel current density (top right), plasma pressure (p, lower right) for the DIII-D 113317 equilibrium, and the finite element mesh (lower left) used for the NIMROD computations.

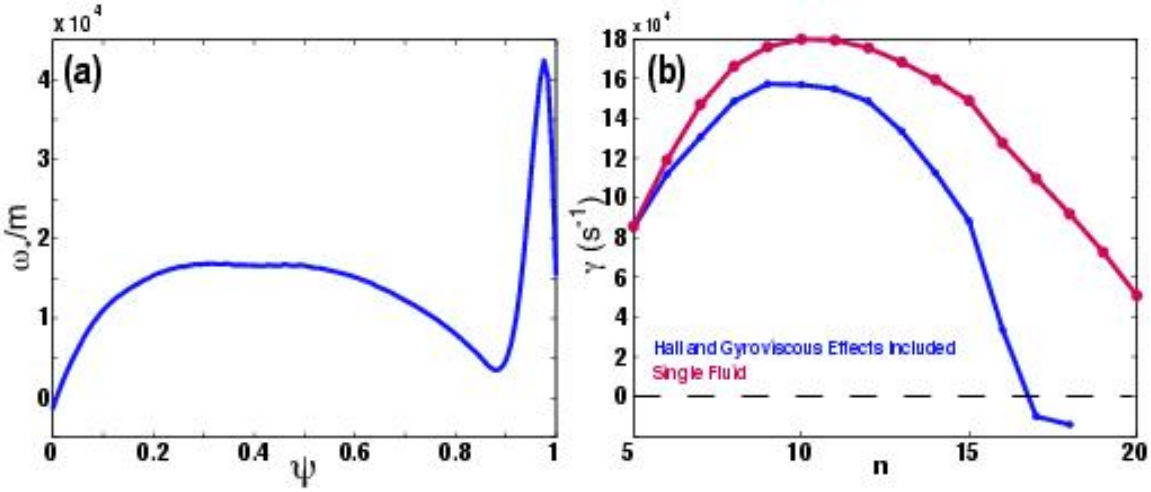

Figure 1.2. Electron drift frequency divided by poloidal mode number *m* (a) and linear growth rates as a function of toroidal mode number *n* for the DIII-D 113317 equilibrium reconstruction. The growth rates for the two-fluid model are shown in blue, and those for the resistive MHD model are shown in red.

1.2 Algorithm development for strong perturbed flows

The NIMROD implementation of the two-fluid equations uses an implicit leapfrog algorithm [Sovinec, C.R., *et al*, J. Phys.: Conference Series **16**, 25 (2005)] where advection is treated implicitly for each step of the leapfrog. The algorithm produces very little numerical dissipation, which is usually beneficial for modeling high-temperature plasmas, but overshoot associated with strong flow perturbations has been problematic for our ELM computations. To provide the benefits of an upwinding algorithm in the implicit computation, a nonlinear artificial diffusivity has been developed. In the continuity equation, for example, the artificial particle flux has the form

$$-f\left(\frac{\Delta t\,\mathbf{V}\cdot\nabla n}{n}\right)^2\left(\frac{A_e}{\Delta t}\right)\frac{\mathbf{VV}}{V^2}\cdot\nabla n \qquad (1)$$

where **V** is the flow velocity, n is the number density, A_e is the element area, and Δt is the time-step. The coefficient f is a user-specified factor. This diffusivity scales numerically as $\Delta t \cdot A_e$, the squared nonlinear factor makes it significant only in the vicinity of large propagating gradients, and the particle flux is along the direction of flow. The implementation is implicit to avoid numerical instabilities with the rest of the time-advance.

To examine the numerical properties of implicit advection with and without the nonlinear diffusivity, we consider the advection of a square pulse. The computations shown in Fig. 1.3 have 10 biquartic elements along the direction of inhomogeneity, which is periodic, and the spatial scale of the jump in the initial conditions is as small as possible. (Only nodal data is plotted, and the quartic polynomials for the initial state—light green trace—have overshoot at the top of the step.) The computation is run 40 steps at a flow-CFL number of unity with and without the nonlinear diffusivity, and the results from all 40 steps are plotted in Fig 1.3 for both cases. The improvement with the nonlinear diffusivity is dramatic and leads to far less spreading than another case (not shown) run with comparable but uniform diffusivity.

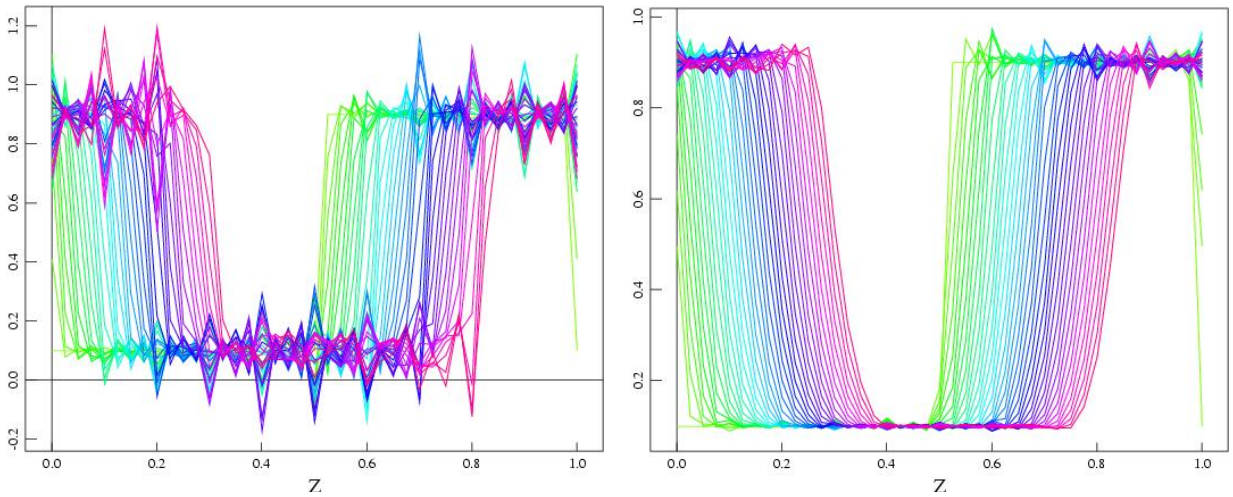

Figure1.3. Passive advection of a square pulse without (left) and with (right) the nonlinear diffusivity of Eq. (1).

The new artificial diffusivity is presently being applied to the evolution of number density and temperature in a nonlinear ELM computation that is based on a realistic DIII-D equilibrium. A pair of implementation errors ('bugs') became evident when running the large parallel computation. These errors have been corrected, and the numerical parameters are being tuned for the ELM computations.

1.3 Nonlinear MHD computations with equilibrium

Nonlinear ELM computations with the requisite 40+ toroidal Fourier components have already been performed with the NIMROD code, albeit with the resistive MHD model. The temporal evolution of the energy spectrum for the DIII-D 113317 equilibrium was presented in the Q2 milestone report. Here, we present new results with a more limited spectrum that include toroidal flow. The flow profile has constant value across the core plasma and a linearly decreasing flow with magnetic flux from ψ=0.85 to ψ=1.0, as shown in Fig. 1.4a. The value of the flow at the magnetic axis is 1×10^5 m/s, which is experimentally relevant. Linearly, the growth rates of the ELMs increase by approximately 20% when this flow profile is added, and there are no qualitative changes in the spectrum. The linear eigenfunctions show a resonance effect between the mode frequency and the flow frequency as indicated in Fig. 1.4c. Nonlinearly, the effects of toroidal flow shear are readily apparent. There is a marked decrease in the amplitude of the perturbation as it extends from the original location of the pressure pedestal (Fig. 1.5). The filaments that easily propagate toward the wall in the static equilibrium are sheared by the flow and do not propagate very far into the vacuum region.

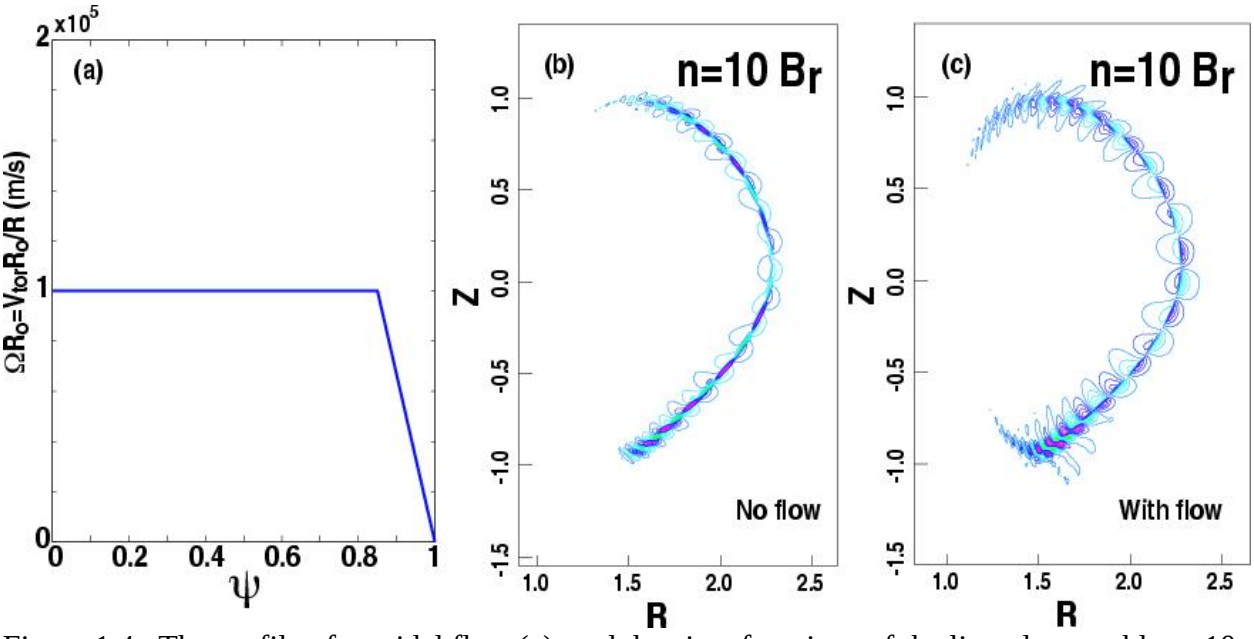

Figure 1.4. The profile of toroidal flow (a), and the eigenfunctions of the linearly unstable n=10 mode without (b) and with (c) sheared toroidal flow.

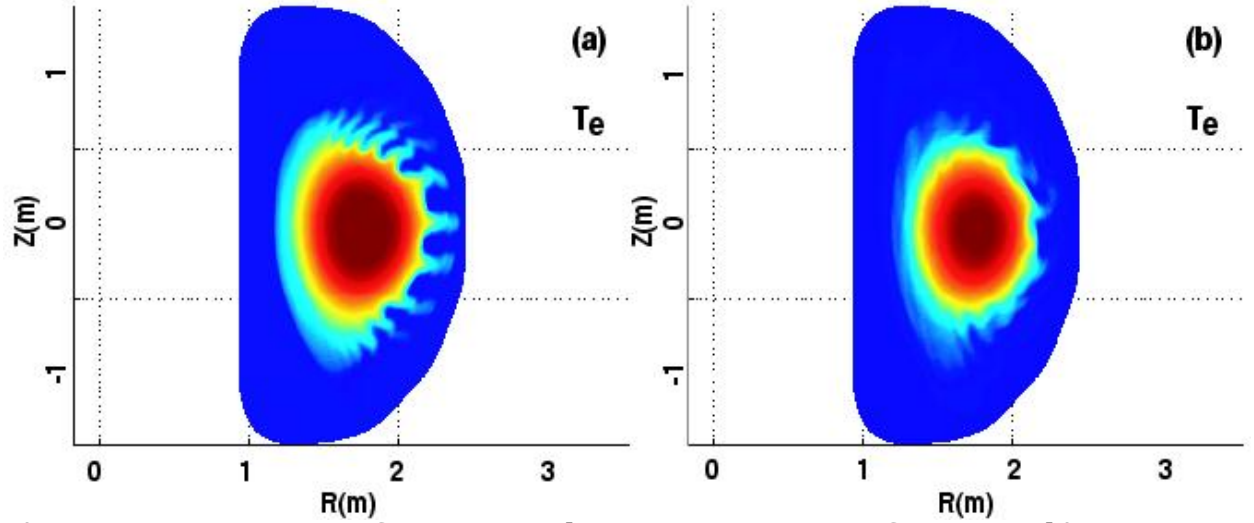

Figure 1.5. Contours of constant electron temperature from a nonlinear computation of an unstable ELM without (a) and with (b) sheared toroidal flow.

Section II. Studies with the M3D Code

In this quarter we prepared for large scale 40+ toroidal mode simulations. The initial simulations are being tried on the shared memory SGI machines: the 32 processor mhd.pppl.gov at PPPL and the 256 processor ram.ccs.ornl.gov. The shared memory M3D code version will also be used to initialize MPP runs which are planned for seaborg.nersc.gov. The shared memory version reads an EQDSK file and produces a mesh. The mesh and equilibrium data are written out in a suitable file format which is used to initialize the MPP version.

An upwind advection algorithm was introduced in M3D to prevent negative density, which can occur when there is strong advection of the density pedestal. The following simulations benefited from the use of upwinding.

We compared simulations of two similar DIII-D EIT equilibria, g113207 and g113317. As before, simulations were done in an outer annulus of plasma, from normalized radius $\rho = 0.8$ to the wall, where $\rho = \sqrt{(\psi - \psi_{axis})/(\psi_{separatrix} - \psi_{axis})}$. The initial density profiles are shown in Fig. 2.1.

The edge density is somewhat lower for case g113207. In the initial EQDSK file, the density is only given out to the separatrix. The density was extended out to the wall by assuming that the density in the open flux surface region is constant and equal to its value at the separatrix.

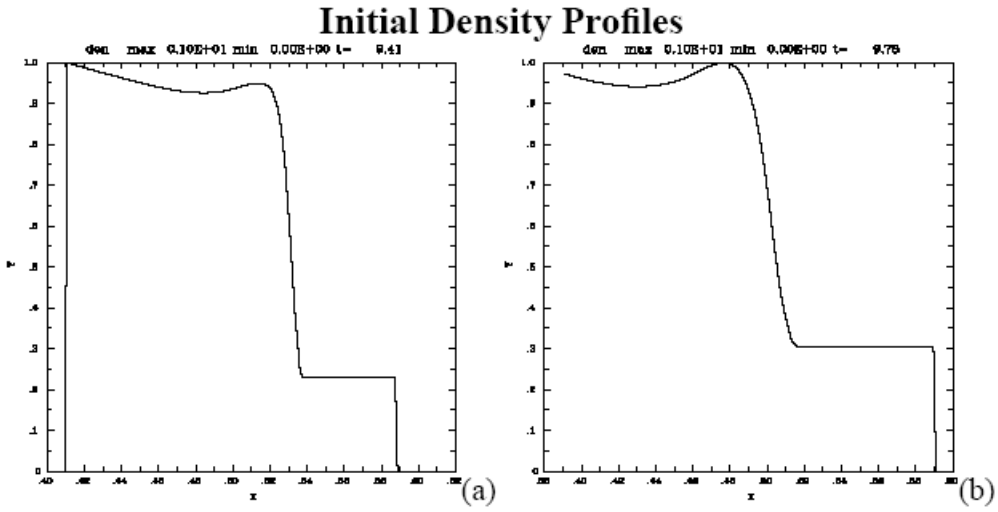

Figure 2.1 (a) initial density profile along the major radius of g113207(b) initial density profile of g113317

The initial pressure profiles are shown in Fig. 2.2. The pressure pedestal is somewhat higher for case g113207.

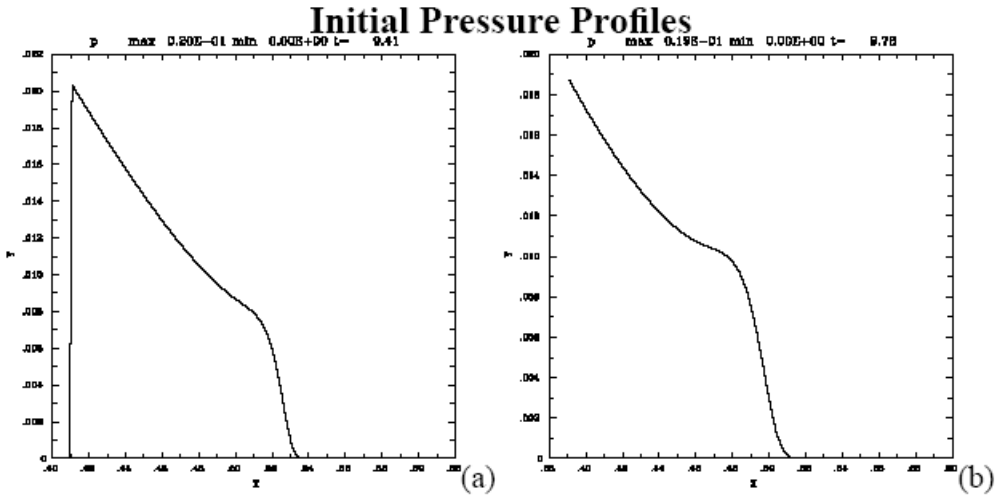

Figure 2.2 (a) initial pressure profile along the major radius of g113207 (b) initial pressure profile of g113317

The initial states were perturbed and a single *n=10* mode was obtained. In case g113207, the growth rate was $1.45\ [\tau_A]^{-1}$ where $[\tau_A] = R/V_A$, R is the major radius, V_A is the Alfvén speed. In case g113317, the growth rate was $1.51\ [\tau_A]^{-1}$. This was used to initialize nonlinear runs with *n= 0, 5, 10, 15, 20.* In the linear and nonlinear runs, $S = \tau_{resistive}/\tau_A = 10^6$, and the Prantl number was *10.*

Nonlinear pressure contours are shown in Fig. 2.3. The pressure is shown at almost the same time: g113207 at $t = 36\ \tau_A$ and g113317 at $t = 37\ \tau_A$. The pressure perturbations appear larger in g113207.

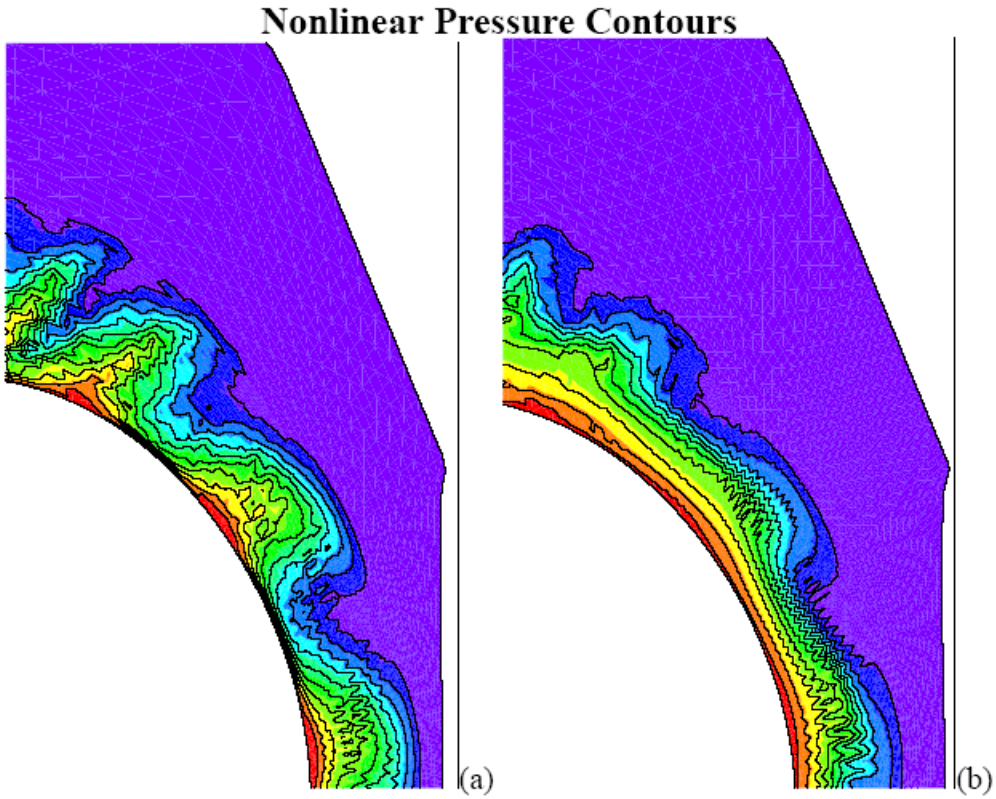

Figure 2.3(a) nonlinear pressure contours in the plane $\phi=0$ of g113207 at $t = 36\ \tau_A$ (b) nonlinear pressure contours of g113317 at $t = 37\ \tau_A$.

The nonlinear pressure profiles are shown in Fig. 2.4

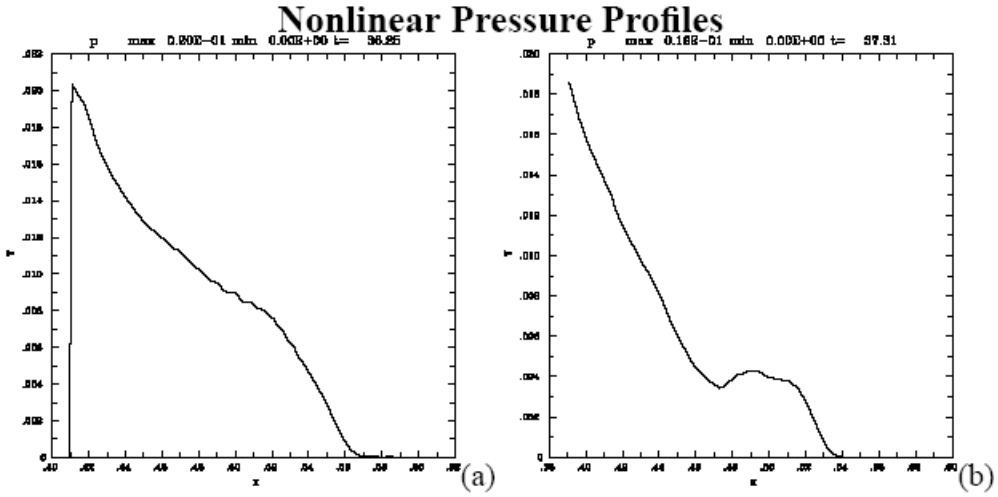

Figure 2.4 (a) nonlinear pressure profile along the major radius of g113207 at $t = 36\ \tau_A$ (b) nonlinear pressure profile of g113317 at $t = 37\ \tau_A$

The nonlinear density profiles are compared in Fig. 2.5. Again the density perturbations are bigger for g113207. It is remarkable that there is a large density ejected all the way out to the wall, even though the pressure is low in the that region.

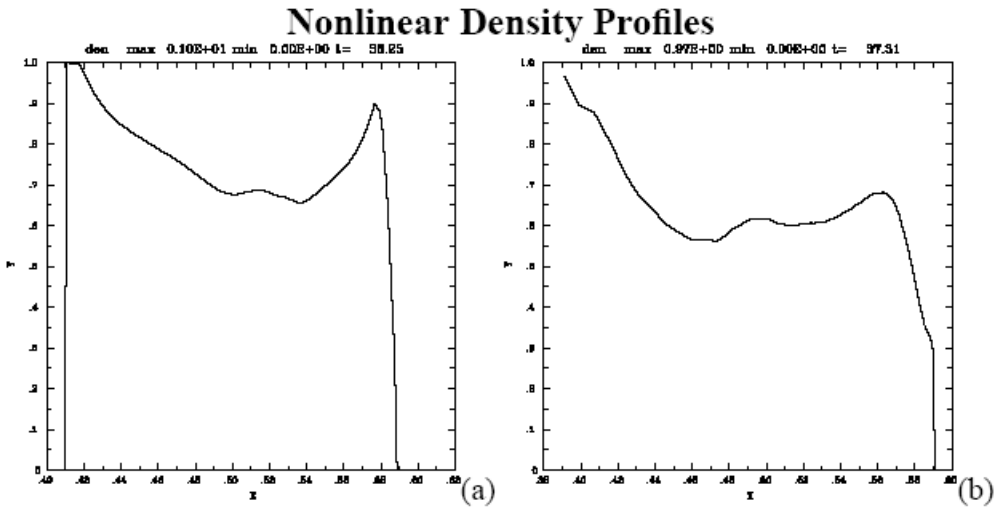

Figure 2.5(a) nonlinear density profile along the major radius of g113207 at $t = 36\ \tau_A$ (b) nonlinear density profile of g113317 at $t = 37\ \tau_A$

The nonlinear density contours also show how density is strongly advected to the wall, and that the effect is stronger in g113207. According to the initial density profiles, g113317 might have been expected to be more unstable. The nonlinear effect might be stronger in g113207 because in that case the density in the edge region is somewhat lower. Perhaps the lower inertia of the edge region causes the nonlinear modes to grow to larger amplitude.

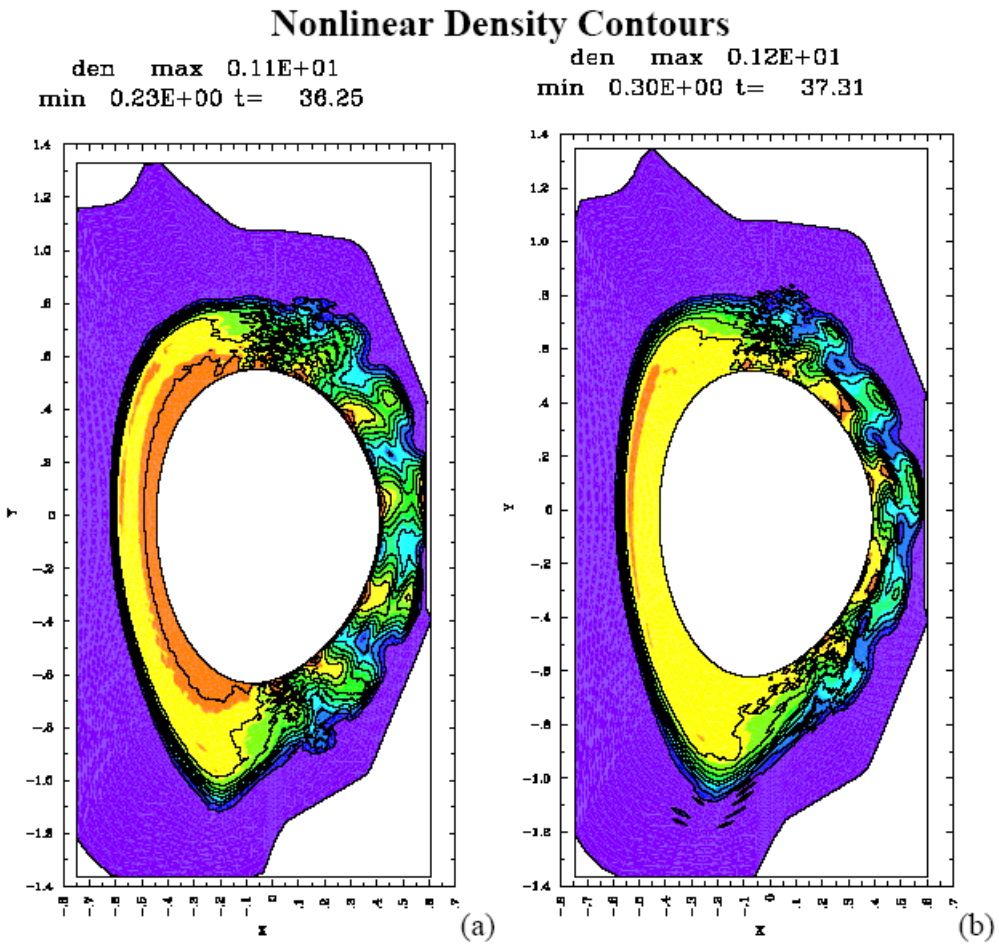

Figure 2.6 (a) nonlinear density contours in the plane $\phi=0$ of g113207 at $t = 36\ \tau_A$ ((b) nonlinear density contours of g113317 at $t = 37\ \tau_A$.

Section III. Summary

The Q3 ELM milestones have been successfully completed with contributions utilizing both the NIMROD and M3D codes. The NIMROD team has implemented the two-fluid effects of the Hall term and gyroviscosity and have verified that these are stabilizing at high *n*-values. This is in qualitative agreement with M3D results discussed in the Q1 milestone report. Both NIMROD and M3D have addressed the problem of the density becoming negative in nonlinear simulations and have implement improved numerical algorithms to prevent this. The effect of sheared toroidal flow has been studied with the NIMROD code. This has the effect of decreasing the amplitude of the perturbation nonlinearly. The M3D code has focused on comparing the two equilibrium that were studied with the NIMROD code in the Q2 milestone report. They found that the equilibrium g113207 had a larger linear growth rate than did g113317, in qualitative agreement with what was reported in the NIMROD studies. They were able to simulate both of these case well into the nonlinear regime and found that the density ejection was also greater for the g113207 equilibrium. Both NIMROD and M3D are in a position to perform meaningful 40+ mode simulations as a result of these preparatory studies.